Journal of
Materials Chemistry B

Materials for biology and medicine

Accepted Manuscript

This article can be cited before page numbers have been issued, to do this please use: J. K. Oh, K. Bairagi, M. Shamekhi, I. Tountas, N. Letourneau, G. Peslherbe and A. Piekny, *J. Mater. Chem. B*, 2025, DOI: 10.1039/D5TB00734H.

ROYAL SOCIETY OF CHEMISTRY

rsc.li/materials-b

View Article Online
DOI: 10.1039/D5TB00734H

Development of Dual Acid/Visible Light-Degradable Core-Crosslinked Nanogels with Extended Conjugate Aromatic Imines for Enhanced Drug Delivery

Kadambari Bairagi,[a] Mehdi Shamekhi,[b,c] Ioanna Tountas,[d] Natasha Letourneau,[d] Gilles H. Peslherbe,[a,b,c] Alisa Piekny,[d] Jung Kwon Oh[a]*

[a] Department of Chemistry and Biochemistry, Concordia University, Montreal, Quebec, Canada H4B 1R6

[b] Department of Physics, Concordia University, Montreal, Quebec, Canada H4B 1R6

[c] Center for Research in Molecular Modeling, Concordia University, Montreal, Quebec, Canada H4B 1R6

[d] Department of Biology, Concordia University, Montreal, Quebec, Canada H4B 1R6

Emails: john.oh@concordia.ca

ABSTRACT

The development of stimuli-responsive amphiphilic block copolymers and their nanoassemblies/nanogels integrated with degradable covalent chemistry undergoing chemical transition has been extensively explored as a promising platform for tumor-targeting controlled/enhanced drug delivery. Conjugate aromatic imine bond is unique to respond to both acidic pH through acid-catalyzed hydrolysis and visible light through photo-induced E/Z isomerization, thus allowing for dual acid/light response with a single conjugate aromatic imine bond. Herein, we report a robust strategy to fabricate well-defined core-crosslinked nanogels bearing extended conjugate aromatic imine linkages, exhibiting controlled degradation in response to dual acidic pH and visible light. The approach utilizes the pre-crosslinking of a poly(ethylene glycol)-based block copolymer bearing reactive imidazole pendants with a diol crosslinker bearing extended conjugate aromatic imine, followed by the mechanical dispersion of

View Article Online
DOI: 10.1039/D5TB00734H

the formed crosslinked polymers in aqueous solution. The fabricated core-crosslinked nanogels with the hydrodynamic diameter of 119 nm are non-cytotoxic, colloidally stable, and able to encapsulate cancer drug curcumin. They exhibit controlled/enhanced release of encapsulated curcumin in acidic pH of 5 and upon irradiation with visible light (λ = 420 nm) and promisingly accelerated and synergistic release with their combination. Furthermore, curcumin-loaded nanogels reduce cell viability in a controlled manner, unlike the free drug. This simplified yet efficient synthetic approach paves the way for the development of smart nanocarriers with potential applications in controlled drug release and cancer therapy.

INTRODUCTION

Development of well-defined amphiphilic block copolymers (ABPs) and their nanoassemblies has emerged as a promising platform for effective intracellular delivery of anticancer therapeutics to tumors.[1-6] They consist of hydrophobic cores, enabling the encapsulation of hydrophobic drugs and hydrophilic corona endowing them with biocompatibility and structural stability.[7] After being intravenously administered, the nanoassemblies extravasate into tumor tissues primarily through the Enhanced Permeability and Retention (EPR) effect.[8-15] Following endocytosis to cancer cells, they are expected for the controlled release of anticancer drugs. However, conventional nanoassemblies present a critical drawback of the uncontrol over the release of therapeutics from conventional nanocarriers in tumor sites.

To overcome this drawback, stimuli-responsive degradation (SRD) has been integrated in the design of ABPs and their nanoassemblies.[16-21] SRD-exhibiting nanoassemblies have been designed with degradable (or labile) covalent bonds, which are cleaved in response to stimuli, preferably endogenous stimuli found cellular environments.[22-24] The degradation causes the disintegration of nanoassemblies, leading to controlled/enhanced release of encapsulated drugs, thus improving the biodistribution of small drug molecules thereby enhancing therapeutic efficacy and minimizing off-target cytotoxicity. Acidic pH is a typical endogenous stimulus because of pH = 6.5-6.9 in tumoral extracellular cellular compartment and pH = 4.5-5.5 in endo/lysosomes.[25-27] In addition to endogenous acidic pH stimulus, light is considered as a

View Article Online
DOI: 10.1039/D5TB00734H

promising exogenous stimulus to achieve on-demand delivery. Typically, imine, acetal and ketal groups as acid-labile linkages[28-35] and o-nitrobenzyl and coumarin dimer groups as photo-cleavable linkages[36-38] have been incorporated into ABP-based nanoassemblies for single stimulus acid- and light-responsive degradation and response. Moreover, a combination of two distinct linkages, typically including o-nitrobenzyl group (light-responsive) with β-thioester,[39] acetal,[40] and imine[41] groups (acid-responsive), has been formulated to achieve dual acid/light-response. Despite these advances, the conventional strategies could increase synthetic complexity, limit scalability, or cause instability issues. Our recent proof-of-concept studies demonstrate the versatility of our approach exploring single conjugate benzoic imine chemistry that enables dual response to acidic pH through acid-catalyzed hydrolysis and UV light through photo-induced E/Z isomerization.[42] However, the approach could be limited for tumor-targeting drug delivery because conjugate benzoic imine bond has its main absorption in UV region which is harmful to tissues. We have envisioned that extending the conjugation of benzoic imine bond can enhance its light absorption toward visible light region. To prove, we have explored an advanced approach that centers on the integration of extended conjugate benzoic imine bond into SRD-ABP-based nanoassemblies to achieve dual acidic pH/visible light response.

Another drawback of conventional nanoassemblies involves their nature of self-assembly through physical entanglement of ABPs in aqueous solution. Upon dilution in blood (4 L), they could be destabilized or disintegrated to the corresponding unimers, causing undesired premature release of drug molecules during blood circulation. To circumvent this drawback, stimuli-responsive degradable core-crosslinked nanoassemblies have been developed.[43-45] They endow structural stability upon dilution, while they facilitate the enhanced release of encapsulated drugs in response to endogenous or exogenous stimulus. A prevalent approach to fabricate core-crosslinked nanoassemblies (or nanogels) is called *in situ* crosslinking. This approach involves the fabrication of aqueous nanoassemblies of reactive ABPs bearing pendant functional groups, followed by their crosslinking induced with external crosslinkers. Click-type reactions such as azide-alkyne cycloaddition,[46-48] conjugation,[49-52] and *in situ* imine formation[53-56] allowed for the fabrication of reduction or acid-degradable core-crosslinked nanogels labeled with disulfide,[47, 48, 51, 52] imine,[53-56] and ketal/acetal[46, 49, 50] linkages. This approach has been proved to be effective; however, when hydrophobic crosslinkers are required for use, this approach remains a critical

View Article Online
DOI: 10.1039/D5TB00734H

challenge due to their limited solubility in aqueous dispersion of nanoassemblies. We have recently explored an alternative, but robust approach that centers on pre-crosslinking of a reactive ABP with a crosslinker in organic solvent, followed by the mechanical dispersion of the formed crosslinked polymers in aqueous solution, yielding well-defined core-crosslinked nanogels. This approach has allowed for the precise control over sizes and functionalities of SRD-exhibiting nanoassemblies with varying ratios of ABP/solvent and reactive functional groups.

In this work, we explored the robust pre-crosslinking dispersion approach to fabricate colloidally stable, core-crosslinked nanogels exhibiting dual acid/visible light response with a single extended conjugate aromatic imine bond (Scheme 1). A diol bearing extended conjugate benzoic imine bond (M3) was newly synthesized as an effective crosslinker for a well-defined PEG-based ABP bearing reactive imidazole pendants (PEG-b-PCIMA). The formed crosslinked polymers (P-Im3-DMSO) were mechanically dispersed in aqueous solution, yielding well-defined core/shell nanogels (P-Im3-Aq) with hydrophobic crosslinked cores, surrounded with hydrophilic PEG corona. They were characterized for dual acid/visible light-responsive degradation through acid-catalyzed hydrolysis and photo-induced E/Z isomerization, confirmed by spectroscopic and computational studies. Further, curcumin-loaded nanogels (P-Im3-Aq/Cur) were evaluated for the uptake and release of encapsulated curcumin, which is an anticancer drug, in HeLa cells.

View Article Online
DOI: 10.1039/D5TB00734H

Scheme 1. A robust approach exploring pre-crosslinking and dispersion techniques that allow for the fabrication of colloidally-stable, core-crosslinked nanogels exhibiting dual acid/visible light response with a single extended conjugate aromatic imine bond, exhibiting controlled/enhanced release of encapsulated Cur drug inside cancer cells. The nanogels are predicted to enter cells via endocytosis, where they can release Cur in the lower pH environments and/or after fusion to form the endo/lysosome, and exposure to light.

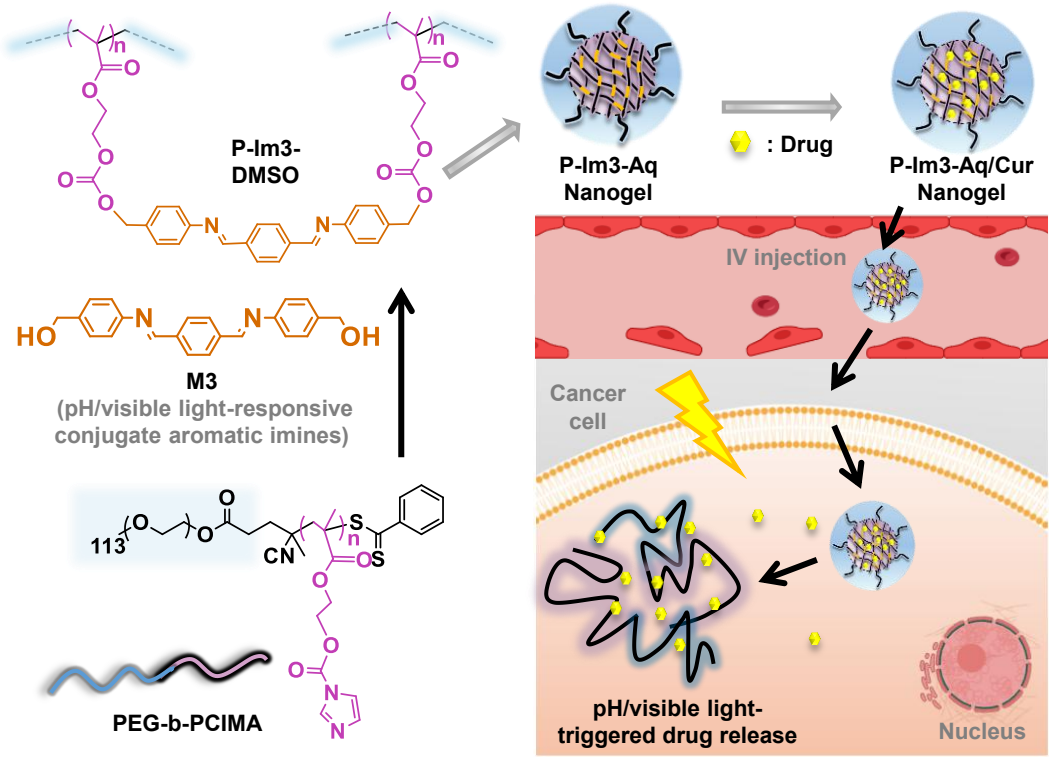

EXPERIMENTAL

Instrumentation. ^{1}H NMR spectra were recorded on a 500 MHz Varian spectrometer. $CDCl_3$ singlet at 7.26 ppm and DMSO-d_6 quintet at 2.5 ppm were selected as reference standards. Exact mass of M3 was analyzed by High Resolution Mass Spectroscopy using a Thermo LTQ Orbitrap Velos mass spectrometer equipped with a heated electrospray ion source. A full MS spectrum (m/z 150-600) was acquired in the Orbitrap at positive mode at a resolution of 100000. Fourier-transform infrared (FT-IR) spectra were collected on a Thermo Scientific

View Article Online
DOI: 10.1039/D5TB00734H

Nicolet iS5 spectrometer with an iD5 attenuated total reflection (ATR) accessory. UV/vis spectra were obtained using an Agilent Cary 60 spectrometer with a 1 cm quartz cuvette. The hydrodynamic diameter and size distribution of aqueous nanogels were analyzed by dynamic light scattering (DLS) using a Malvern Nano S ZEN1600 system, equipped with a 633 nm He-Ne laser, at a fixed scattering angle of 175° and a temperature of 25 °C.

Light-responsive experiments were conducted with a PR160L-440nm Gen 2 LED lamp (Kessil, USA) at λ = 440 nm (60 mW/cm²) and a MAX-302 xenon arc lamp (Asahi Spectra) at λ = 420 nm (1.7 mW/cm²) at a distance of 15 cm from their light sources.

Transmission Electron Microscopy (TEM) images were acquired using a FEI Tecnai G2 F20 200 kV Cryo-STEM with Gatan Ultrascan 4000 4kx4k CCD Camera System Model 895. For negative staining, a 1% phosphotungstic acid solution was prepared by dissolving 5 mg of phosphotungstic acid in 0.5 mL of deionized water, followed by the addition of 5 µL of 1 M sodium hydroxide and filtration through a 0.45 µm PES membrane. Aqueous dispersions (5 µL) were drop-cast onto a 300-mesh copper TEM grid and left undisturbed for 2 min. Excess liquid was blotted with filter paper before applying a drop of stain. The grid was blotted again and dried under a fume hood before imaging.

Differential scanning calorimetry (DSC) analysis was conducted to investigate thermal properties including glass transition temperature (T_g) of crosslinked polymers with a TA Instruments DSC Q20 Differential Scanning Calorimeter. Polymer samples were dried in vacuum oven for 24 hrs to remove residual solvents. Temperature ranged from −80 to 200 °C with heating and cooling cycles at a rate of 10 °C/min (cycles: cool to −80 °C and heat up to 200 °C (1st run), cool to −80 °C and heat up to 200 °C (2nd run), and cool to 25 °C. T_g values were determined from the 2nd heating run. Thermogravimetric analysis (TGA) was conducted with a TA Instruments Q50 Analyzer. Dried polymer samples (10 mg) were placed in a platinum pan inside a programmable furnace and then heated from 25 to 800 °C at a heating rate of 20 °C/min under nitrogen flow.

Materials. 2-Hydroxyethyl methacrylate (HEMA, 99%, purified by passing through a column filled with basic aluminum oxide to remove the inhibitor), 1,1′-carbonyldiimidazole (CDI, 97%), 1,8- diazabicyclo[5.4.0]undec-7-ene (DBU, 98%), 4-(methylamino)pyridine

View Article Online
DOI: 10.1039/D5TB00734H

(DMAP, 99%), 4-cyano-4 (phenylcarbonothioylthio) pentanoic acid (CTA, 97%), 4-aminobenzyl alcohol (ABA, 98%), terephthalaldehyde (TDA, 98%), curcumin (Cur, 99%), methoxy-terminated poly(ethylene glycol) (PEG, MW = 5000 g/mol, dried by an azeotropic distillation with anhydrous toluene prior to use), and 2,2′-azobis(2-methylpropionitrile) (AIBN, 98%) from Sigma-Aldrich and 1-ethyl-3-(3 dimethylaminopropyl) carbodiimide•HCl (EDC) from Matrix Innovation were purchased and used as received. A carbonyl imidazole-bearing methacrylate (CIMA)[40] and a CTA-functionalized PEG (PEG-RAFT)[57] were synthesized as described elsewhere.

Synthesis of M3. ABA (0.73 g, 6.0 mmol) was mixed with TDA (0.40 g, 3.0 mmol) in DMF (7 mL) in an oil-bath preset at 100 °C under stirring for 18 hrs. The resulting mixture was purified by precipitation from cold diethyl ether. The precipitate was dried in a vacuum oven at room temperature for 24 hrs to yield yellow solid. Yield = 0.70 g (67%). ^{1}H NMR (DMSO-d_6, ppm): 8.7 (s, 2H, -N<u>CH</u>C_6H_4<u>CH</u>N-), 8.06 (m, 4H, NCH<u>C_6H_4</u>CHN), 7.32-7.25 (m, 8H, -<u>C_6H_4</u>NCH <u>C_6H_4</u>CHN <u>C_6H_4</u>-), 5.22 (s, 2H, - <u>$C_6H_4CH_2OH$</u>), 4.5 (s, 4H, - <u>$C_6H_4CH_2$</u>OH). ^{13}C NMR (DMSO-d_6, ppm): 159.8, 150.1, 141.3, 138.9, 129.3, 127.8, 63.0. Mass calculated for $C_{22}H_{20}N_2O_2$ $[M+H]^+$: 345.1598 and found: 345.1600.

Synthesis of PEG-b-PCIMA via RAFT Polymerization. CIMA (1 g, 4.5 mmol), PEG-RAFT (0.24 g, 45.6 μmol), and AIBN (3.7 mg, 22.8 μmol) were mixed with anisole (1.7 mL) in a 10 mL Schlenk flask. The mixture was purged with nitrogen for 45 min and then placed in an oil-bath preset at 70 °C to start polymerization. After 3 hrs, the mixture was cooled down to room temperature to stop polymerization. For purification, as-synthesized polymers were precipitated from cold hexane and isolated by vacuum filtration. The procedure was repeated three times and then the polymer was dried in a vacuum oven at 40 °C for 24 hrs.

CDI-Mediated Crosslinking to Fabricate P-Im3-DMSO Crosslinked Polymers. M3 (26 mg, 74.3 μmol, 149 μmol equivalent of OH groups) was mixed with PEG-b-PCIMA (52.5 mg, 3.6 μmol, 149 μmol equivalent of CIMA units) and DBU (4.5 mg, 30 μmol) in DMSO (6 mL) under stirring at room temperature for 24 hrs. The formed crosslinked polymers were precipitated from cold diethyl ether and then dried in a vacuum oven at 40 °C for 24 hrs.

View Article Online
DOI: 10.1039/D5TB00734H

Fabrication of Aqueous P-Im3-Aq Nanogels by Pre-crosslinking Dispersion Approach. Typically, to fabricate P-Im3-Aq at 0.31 mg/mL, M3 (1.7 mg, 5 μmol) was mixed with PEG-b-PCIMA (3.5 mg, 0.2 μmol) and DBU (0.3 mg, 2 μmol) in DMSO (2 mL) under stirring at room temperature for 24 hrs. Deionized water (10 mL) was then added dropwise at 60 mL/hr using a syringe pump under stirring. The resulting dispersion was dialyzed against water (1 L) using a dialysis tubing with MWCO = 11–13 kDa for 24 hrs and then filtered with a 0.45 μm PES filter**.**

The similar procedure was examined with the varying amounts of DMSO and water to investigate DMSO/water ratio (called P-Im3-Aq-A, B, and C) as well as the varying amounts of PEG-b-PCIMA and M3 to investigate CI/OH mole equivalent ratio (called P-Im3-Aq-D and E). The recipes are summarized in Table S1.

Conventional *In Situ* Crosslinking Approach in Attempt to Fabricate Aqueous Crosslinked Nanoassemblies. Typically, deionized water (10 mL) was added dropwise to an organic solution consisting of M3 (4.8 mg, 14.0 μmol) and PEG-b-PCIMA (10 mg, 0.7 μmol) in DMSO (2 mL) at a rate of 60 mL/hr using a syringe pump under magnetic stirring at room temperature. The resulting dispersion was dialyzed against water (1 L) using a dialysis tubing with MWCO = 11–13 kDa for 24 hrs. DBU (0.8 mg, 5.6 μmol) was added, and the resulting mixture was stirred at room temperature for another 24 hrs.

Acid-Responsive Degradation of Aqueous Nanoassemblies. Aqueous P-Im3-Aq nanogels (2 mL, 0.31 mg/mL) were mixed with 0.2 M sodium acetate buffer solution at pH = 5.0 (2 mL) under stirring at room temperature. Aliquots were taken for DLS and TEM analysis.

Acid-Responsive Degradation of M3 in DMSO using ^{1}H NMR Spectroscopy. To investigate acid-catalyzed hydrolysis of benzoic imine bonds, M3 (10 mg, 30 μmol) was dissolved in DMSO-d_6 (1 mL) and then mixed with HCl (5 μL, 60 μmol) at a 1/1 mole equivalent ratio of C=N/H^+ (equivalent to pH = 1.2 or pD = 1.6, calculated using pD = pH + 0.4). ^{1}H NMR spectra of the resulting mixtures were recorded for given time intervals. Similar procedure was used for P-Im3-DMSO polymer, except with the use of P-Im3-DMSO (10 mg) swollen in DMSO-d_6 (1 mL).

Light-Responsive Degradation of Aqueous Nanoassemblies. Aqueous P-Im3-Aq nanogels (3 mL) in a quartz cuvette were exposed upon the irradiation of visible light with λ =

View Article Online
DOI: 10.1039/D5TB00734H

440 nm (60 mW/cm²). Their UV/Vis spectra were recorded to follow change in absorbance at λ = 355 nm.

Light-Responsive Degradation of M3 in DMSO via UV/Vis Spectroscopy. A solution of M3 (31 μg) dissolved in DMSO (3 mL) at 30 μM in a quartz cuvette was exposed upon the irradiation of visible light with λ = 440 nm (60 mW/cm²). Their UV/Vis spectra were recorded to monitor change in absorbance at λ = 355 nm over irradiation time.

Computational Details. Density functional theory (DFT) calculations with the range-separated hybrid exchange-correlation (XC) functional based on B97 exchange (ωB97XD) are performed to evaluate the structural and electronic properties of the molecular structures.[58] The molecular geometries were fully optimized at the ωB97XD level of theory along with the 6–311++G(d,p) split-valence triple-ζ Pople basis set[59] Vibrational frequency analysis was carried out to confirm that each configuration was a minimum on the potential energy surface (zero imaginary frequencies), and thermodynamic properties were evaluated within the rigid-rotor harmonic oscillator approximation. The STQN method was used to locate the transition states for the interconversion of structures. Three structure specifications are required in this method: the reactants (EE for EE → EZ and EZ for EZ → ZZ), the products (EZ for EE → EZ and ZZ for EZ → ZZ), and an initial guess for the transition state structure. The energies of the highest occupied molecular orbital (HOMO), lowest unoccupied molecular orbital (LUMO), and the electronic bandgap (E_g) between these orbitals were determined through analysis of frontier molecular orbitals (FMOs). The energies of the singlet-excited-state transitions were calculated using time-dependent DFT (TD-DFT) for optimized molecular structures. We note that ωB97XD is a reliable XC functional to accurately capture the UV/Vis light absorption spectra for the structures due to the partitioning of short and long range components, compared to traditional hybrid XC functionals such as the Becke three-parameter hybrid methods with the Lee–Yang–Parr correlation functional (B3LYP).[60] For all the calculations the Gaussian 16 (revision C.01) software package of programs was used along with the GaussView6 interface for structure and orbital manipulations.[61] The enthalpy and free energy of the reaction was calculated as summarized in Table S2.

Preparation of Cur-Loaded Nanogels. An organic solution of Cur (1 mg) dissolved in DMSO (2 mL) was added dropwise to aqueous P-Im3-Aq nanogel dispersion (0.31 mg/mL, 12

View Article Online
DOI: 10.1039/D5TB00734H

mL) under stirring for 1 hr. The resulting mixture was transferred to dialysis tubing with MWCO = 11–13 kDa for dialysis against water (1 L) for 24 hrs. The dispersion was filtered through a 0.45 μm PES filter to remove unencapsulated (free) Cur, yielding aqueous Cur-loaded nanogels (P-Im3-Aq/Cur) at 0.27 mg/mL.

To determine the loading level of Cur in nanogels, a series of solutions containing different amounts of Cur in a mixture of THF and water (1/1 v/v) were prepared, and their UV/Vis spectra were recorded to determine the extinction coefficient of Cur at λ = 430 nm. Then, aliquots of P-Im3-Aq/Cur (1 mL) were mixed with THF (1 mL) and filtered through a 0.45 μm PTFE filter. UV/Vis spectrum of the filtrate was recorded to quantify encapsulated Cur using the pre-determined extinction coefficient**.**

Stimuli-Responsive Release of Cur from P-Im3-Aq/Cur Nanogels. For light-responsive release, aliquots of P-Im3-Aq/Cur (2 mL) were irradiated with visible light with λ = 420 nm (1.7 mW/cm²). Other aliquots were kept in dark as control. For acidic pH-responsive release, aliquots of P-Im3-Aq/Cur (2 mL) were mixed with 0.2 M sodium acetate buffer solution (2 mL) at pH = 5.0 and 7.4 under stirring. For dual acidic pH/light-responsive release, aliquots of P-Im3-Aq/Cur (2 mL) mixed with 0.2 M sodium acetate buffer solution (2 mL) at pH = 5.0 were exposed to visible light with λ = 420 nm (1.7 mW/cm²) at room temperature under stirring. To determine the %release of Cur from nanogels, UV/Vis spectra of supernatants were recorded for given time intervals and the absorbance at λ = 430 nm was monitored.

Cell Culture. HeLa cervical cancer cells were cultured in DMEM (Dulbecco's modified Eagle's medium) containing 10% CCS (cosmic calf serum) and were kept at 37 °C with 5% CO_2 in a HERAcell Vios 160i incubator (ThermoFisher Scientific).

Viability Assay. HeLa cells were plated at 2.5×10^3 cells per well in a 96-well plate and incubated for 24 hrs in 100 μL of DMEM with 10% CCS for 24 hrs at 37 °C with 5% CO_2. Various concentrations of aqueous P-Im3-Aq/Cur nanogels as well as aqueous P-Im3-Aq nanogels (empty, e.g. Cur-free) and free Cur as controls were added to the cells for 72 hrs. Due to the poor solubility of Cur in aqueous media, aliquots of Cur dissolved in DMSO were diluted with cell culture media to keep DMSO to be as low as 1% for all control samples. Cell viability was measured using the WST-8 proliferation assay kit as per manufacturer's instructions

View Article Online
DOI: 10.1039/D5TB00734H

(Cayman Chemicals). Briefly, the medium containing samples was carefully removed and 100 µL of the prepared colorimetric reagent WST-8 (0.5 mM, 5-(2,4-disulfophenyl)-3-(2-methoxy-4-nitrophenyl)-2-(4-nitrophenyl)-2H-tetrazolium, inner salt, monosodium salt) was added to each well. After 2hrs, aTecan Infinite M200 Pro plate reader was used to measure the absorbance at λ = 450 nm for each well. Wells with untreated cells were measured as a positive control, while WST-8 reagent alone was measured to have a 'blank' reference. Each treatment was replicated 3 times. Cell viability was calculated as the percent ratio of absorbance of mixtures with nanogels to control (untreated cells).

Live Cell Imaging by Fluorescence Microscopy. HeLa cells were plated in DMEM with 10% CCS at $2.5x10^5$ cells/mL in a µ-slide 4-well dish. The cells were treated with 240 µg/mL of P-Im3-Aq/Cur nanogels, 2.72 µg/mL free Cur solution (2.72 µg/mL) or 240 µg/mL of P-Im3-Aq and SYTO Deep Red Nucleic Acid Stain (Thermo Fisher) for 2 hrs at 37 °C with 5% CO_2. Live cells were visualized on a Nikon Ti2 microscope equipped with a Yokogawa CSU-X1 spinning disk, a Gataca Live-SR unit, an Andor Zyla 4.2 (Oxford instruments, UK), 60x/1.45NA PlanApo objective lens and DIC optics. Cur was excited with a λ = 488 nm laser (18% power, 200 ms exposure time), and SYTO Deep Red was excited with a 638 nm laser (10% power, 200 ms exposure time). Images were acquired with Micro-Manager. Images were viewed and analyzed on ImageJ.

RESULTS AND DISCUSSION

Synthesis and UV/Vis Absorption Characteristics of Extended Conjugate Benzoic Imine-Bearing Diol Crosslinker. Figure 1a depicts our approach to synthesize a new diol crosslinker bearing two conjugate benzoic imine bonds (called extended conjugate benzoic imine bonds), labelled as M3. The approach utilizes a facile condensation reaction of an amine group of ABA with two aldehyde groups of TDA at an elevated temperature through the formation of benzoic imine bonds. ^{1}H NMR spectrum in Figure 1b shows the new peak at 8.72 ppm (a) corresponding to imine proton, along with the peak at 4.53 ppm (e) corresponding to methylene protons in benzyl moieties and the peaks at 7.35 ppm (b) and 8.07 ppm (c) corresponding to aromatic protons. Their integrals were quantitative to the numbers of protons. This result,

View Article Online
DOI: 10.1039/D5TB00734H

combined with ^{13}C NMR spectrum (Figure S1) and HR-MS (Figure S2), confirms the successful synthesis of M3.

Given the synthesis of M3, its UV/Vis absorption characteristics was investigated in DMSO and compared with M-HX (a methacrylate bearing a benzoic imine bond)[62] and M2 (a methacrylate bearing a conjugate benzoic imine bond).[42] As seen in Figure 1c, M3 exhibits an extended absorption up to 450 nm, with a distinct absorption at λ = 355 nm corresponding to $n\rightarrow\pi^*$ transition and a secondary absorption at λ = 310 nm attributed to $\pi\rightarrow\pi^*$ transition. Its extinction coefficient at λ = 355 nm was determined to be 32,000 M^{-1} cm^{-1} (Figure S3). Promisingly, its absorption was red-shifted because of the extended benzoic imine conjugation, compared with M2 having its maximum absorption at λ = 285 nm (ε = 20,100 $M^{-1}cm^{-1}$ in DMF) and further to M-HX having its maximum absorption at λ = 255 nm (ε = 2,200 $M^{-1}cm^{-1}$ in DMF).

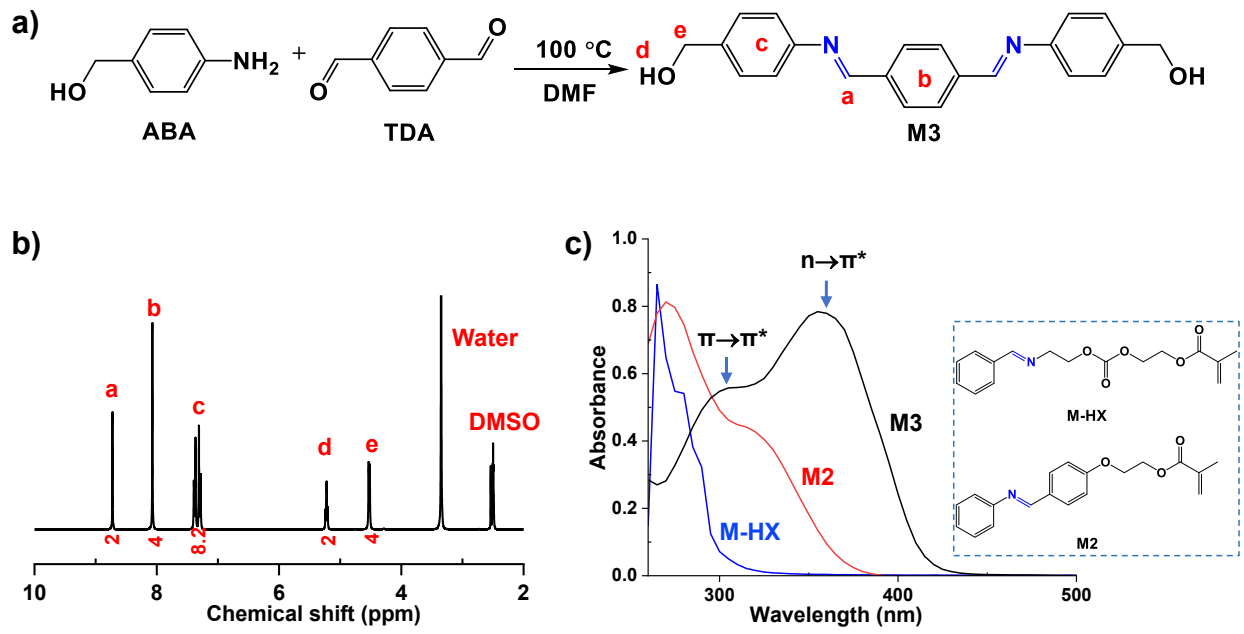

Figure 1. Synthesis of M3 (a diol crosslinker bearing an extended conjugate benzoic imine) by condensation reaction of ABA with TDA in DMF (a), its ^1H NMR spectrum in DMSO-d_6 (b), and its UV/vis spectrum in DMSO, compared with those of M2 (a methacrylate bearing a conjugate benzoic imine bond) and M-HX (a methacrylate bearing a benzoic imine bond) in DMF (c).

View Article Online
DOI: 10.1039/D5TB00734H

Synthesis of Reactive PEG-b-PCIMA Copolymer Bearing Imidazole Pendant. As illustrated in Figure 2a, RAFT polymerization was examined for CIMA in the presence of PEG-RAFT, a PEG-based macro-RAFT mediator, initiated with AIBN in anisole at 70°C, to synthesize a well-defined PEG-based block copolymer bearing reactive imidazole pendants (PEG-b-PCIMA). The conditions include the initial mole ratio of $[CIMA]_0/[PEG\text{-}RAFT]_0/[AIBN]_0 = 100/1/0.5$ with the targeted degree of polymerization (DP) = 100 at complete monomer conversion. The synthesized copolymer was purified by precipitation from hexane to remove unreacted CIMA at 40% conversion. ^{1}H NMR spectrum in Figure 2b shows the presence of PEG at 3.6 ppm and pendant imidazole rings at 7.0-8.2 ppm. Their integral ratio, with the DP of PEG = 113, allows to determine the DP of the PCIMA block to be 41, thus forming PEG_{113}-b-$PCIMA_{41}$.

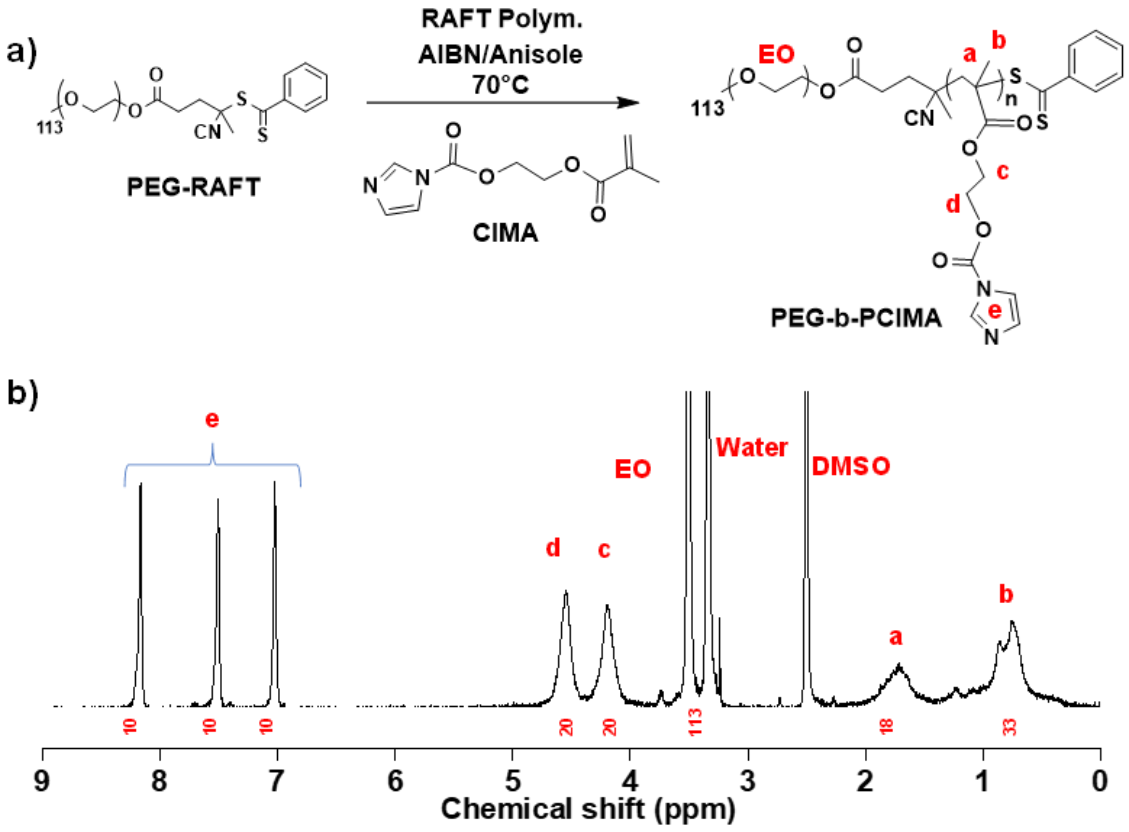

Figure 2. Synthesis by RAFT polymerization (a) and ^{1}H NMR spectrum in DMSO-d_6 of PEG-b-PCIMA block copolymer. Conditions: $[CIMA]_0/[PEG\text{-}RAFT]_0/[AIBN]_0 = 100/1/0.5$; CIMA/anisole (w/w) = 1/0.6.

View Article Online
DOI: 10.1039/D5TB00734H

Studies of CDI-mediated Crosslinking Reaction to Fabricate Crosslinked Polymers. Given the synthesis of well-defined PEG-PCIMA and M3 diol crosslinker, their CDI-mediated coupling reaction between pendant CI groups with OH groups were investigated in an organic solvent (Figure 3a). DMSO was chosen because it was found to be a good solvent to both PEG-PCIMA and M3 precursors. With a choice of CI/OH mole equivalent ratio = 1/1, aliquots of PEG-PCIMA and M3 were mixed in DMSO at 50 mg/mL to induce CDI-mediated crosslinking. The formed PEG-PCIMA/M3 crosslinked polymer (called P-Im3-DMSO) was isolated by precipitation from diethyl ether and then analyzed by solubility, ^{1}H NMR and FT-IR spectroscopies for chemical structure, and DSC and TGA for thermal properties.

The polymer turned out to be insoluble in any organic solvents including DMSO and its gel content to measure insoluble species in DMSO was greater than 84%. Given the polymer being swollen in DMSO-d_6, ^{1}H NMR spectrum in Figure S4 shows no peaks corresponding to protons in copolymer. In addition, ^{1}H NMR spectrum of supernatant in Figure S5 shows two peaks at 7.0 and 7.6 ppm presenting imidazole which could be generated as a side product during CDI-mediated crosslinking. Moreover, its FT-IR spectrum in Figure 3b shows the characteristic C=N stretching vibration at 1620 cm^{-1}, along with C-H stretching vibration at 2800-3000 cm^{-1} and carbonyl vibration at 1700-1750 cm^{-1}. These results confirm the formation of crosslinked polymer network through the formation of carbonate bonds by CDI-medicated crosslinking reaction of PEF-b-PCIMA with M3. The crosslinked polymer had a single glass transition at -21 ° C and a single melting transition at 55.2 °C, by DSC analysis (Figures S6). It also had the temperature at which its mass loses half to be 407 ° C with 15% residue, by TGA analysis (Figure S7).

View Article Online
DOI: 10.1039/D5TB00734H

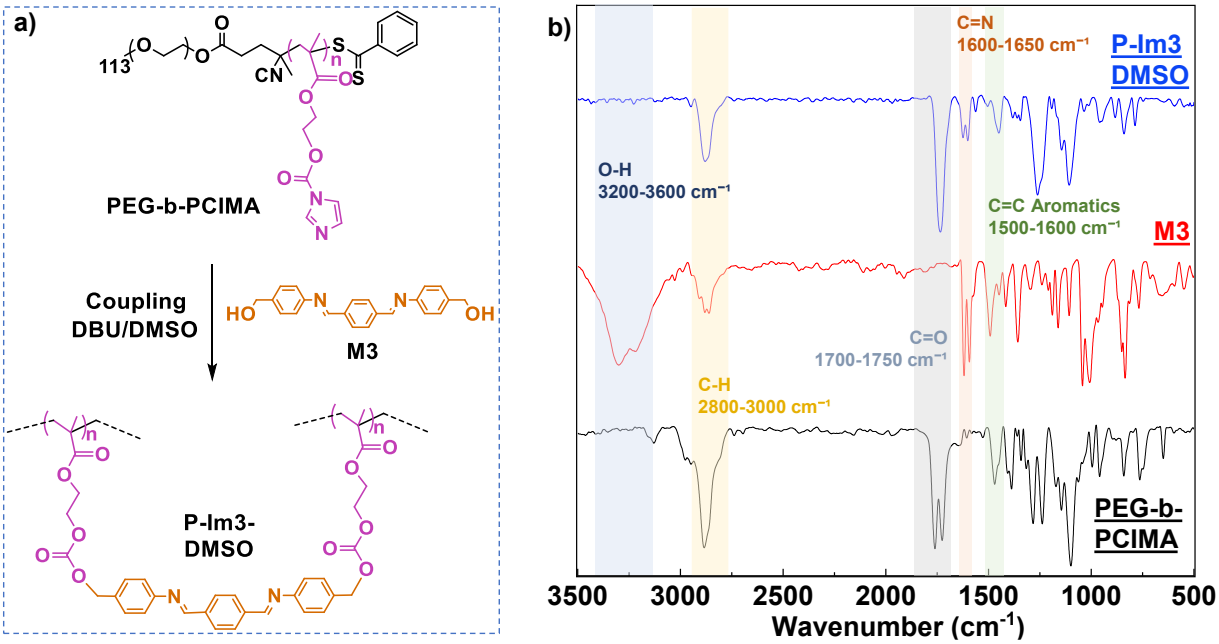

Figure 3. Schematic presentation for CDI-medicated crosslinking reaction of PEG-b-CIMA with M3 diol crosslinker to form cross-linked P-Im3-DMSO polymer network (a) and its FT-IR spectrum, compared with those of M3 and PEG-b-PCIMA precursors (b).

Pre-crosslinking Dispersion Approach to Fabricate Aqueous Crosslinked Nanogels. A new approach centered on pre-crosslinking in a homogeneous solution was explored to fabricate colloidally stable crosslinked nanogels dispersed in aqueous solution. The approach consists of two steps, including i) the synthesis of P-Im3-DMSO crosslinked polymer from a mixture of PEG-b-PCIMA and M3 at CI/OH = 1/1 in DMSO and ii) its spontaneous self-assembly in water to yield nanogel dispersion. Because of the amphiphilic nature of P-Im3-DMSO polymer, the formed nanogels consist of crosslinked hydrophobic cores surrounded with hydrophilic PEG corona in water.

After being purified by dialysis, the resulting dispersion was determined to be 0.31 mg/mL, which is close to that (0.36 mg/mL) in the recipe, suggesting the loss of polymeric species during pre-crosslinking/dispersion process could be negligible. The purified aqueous nanogels were characterized for size and size distribution as well as morphology. As seen in Figure 4a, the nanogels had a diameter of 119 nm and their size distribution appeared to be narrow and

View Article Online
DOI: 10.1039/D5TB00734H

monomodal, based on DLS analysis. No visible aggregates were observed. TEM analysis reveals that they had a diameter 87 ± 21 nm in the dried state, which is smaller than that by DLS analysis (inset in Figure 4a). Furthermore, the nanogels were characterized for UV/Vis absorption characteristics. As compared in Figure 4b, it had an absorption at λ = 355 nm, which is similar to M3 crosslinker, indicating that extended conjugate benzoic imine bonds are intact on the course of the fabrication of nanogels. These results confirm that pre-crosslinking/dispersion approach is robust and enables the fabrication of colloidally stable nanogels in aqueous solution.

Important parameters that significantly influence colloidal stability and sizes were systematically investigated by DLS analysis. Figure 4c shows the change in diameter of P-Im3-Aq nanogels in water. One parameter is CI/OH mole equivalent ratio. When the ratio increased (e.g. decreasing the number of crosslinks), the diameter increased. Another parameter is the amount of PEG-b-PCIMA in DMSO as DMSO/PEG-b-PCIMA v/wt ratio for CDI-mediated crosslinking reaction. The diameter increased with an increasing ratio (e.g. amount of DMSO). These results and trends of change in sizes indicate that the size of core-crosslinked nanogels greatly relies on crosslinking density and thus highly crosslinked networks are likely to produce more compact hydrophobic cores.

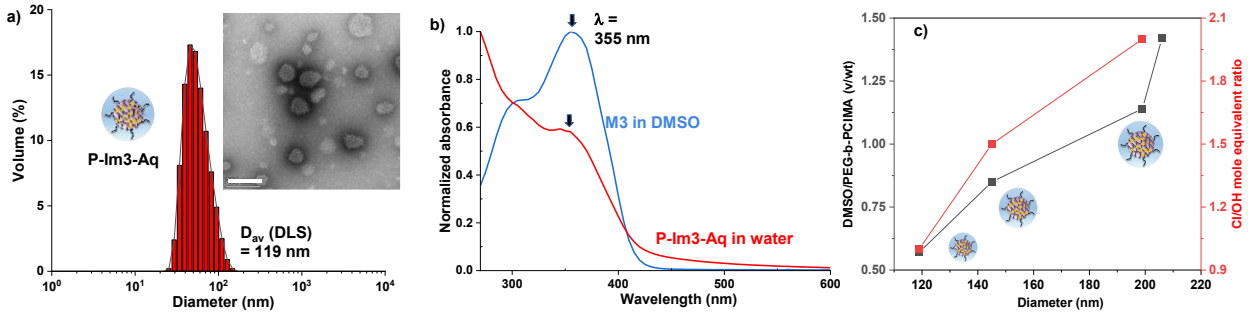

Figure 4. For P-Im3-Aq nanogels in aqueous solution, DLS diagram with inset TEM image (scale bar = 200 nm) (a), UV/Vis spectrum at 0.3 mg/mL, compared with that of M3 in DMSO (30 μM) (b), and evolution of diameter with varying amount of DMSO and CI/OH mole equivalent ratio (c).

In our separated experiment, a conventional *in situ* crosslinking approach was examined in an attempt to fabricate aqueous crosslinked nanoassemblies. The approach involves the

View Article Online
DOI: 10.1039/D5TB00734H

fabrication of aqueous nanoassemblies consisting of PEG-b-PCIMA and M3 through self-assembly, followed by the addition of water-soluble DBU as a catalyst in aqueous solution. The resulting dispersion was white-colored with visible aggregates (Figure S8). The dispersion was subjected to dialysis and filtration to remove significant amount of white aggregates. The resulting dispersion turned out to be blue-tinted with the average diameter of 125 nm by DLS. When being characterized by UV-Vis spectroscopy, the dispersion shows no absorption at λ = 355 nm corresponding to $n \rightarrow \pi^*$ transition, characteristic of M3, in its UV/Vis spectrum. Our attempts with the variation of the amounts of PEG-b-PCIMA and M3 over DMSO and water were not straightforward toward the fabrication of colloidally-stable aqueous dispersion of crosslinked nanoassemblies by this approach.

Studies of Acid-Responsive Degradation and Disassembly. Aqueous P-Im3-Aq nanogels contain extended conjugate benzoic imine bonds in the crosslinks of hydrophobic cores which could be cleaved in an acidic environment. Aliquots of the nanogels were incubated in acidic buffer at pH = 5.0, and their acid-responsive degradation was investigated using DLS and TEM techniques. DLS analysis reveal that their size distribution became multimodal with appearance of large aggregates in 6 hrs of incubation (Figure 5a). TEM analysis further confirms the occurrence of large aggregates (Figure 5b, 5c) and the digital images of the aqueous nanogel dispersion show the change in color from turbid white to visibly clear after 24 hrs of incubation in acidic buffer (Figure 5d, 5e). Further, precipitates were visible in the bottom of the vials. These results could be attributed to the disintegration of P-Im3-Aq nanogel cores via the cleavage of benzoic imine bonds to corresponding aldehyde and amine under an acidic condition.

Further to get insights, acid-responsive degradation of M3 and crosslinked polymer (P-Im-DMSO) through acid-catalyzed hydrolysis of benzoic imine bonds was quantitatively investigated using ^{1}H NMR spectroscopic analysis. First, M3 dissolved in DMSO-d_6 was incubated with HCl (an acid) for 2 hrs. ^{1}H NMR spectrum in Figure 5g shows the disappearance of the peak at 8.6 ppm corresponding to imine proton (a), and appearance of a new peak at 9.2 ppm corresponding to aldehyde proton (b). These changes confirm the cleavage of imine bonds into the corresponding aldehyde and amine precursors through acid-catalyzed hydrolysis (Figure 5f). Their integral ratio allows the %hydrolysis to be 82%. Next, P-Im3-DMSO swollen in DMSO-d_6 was treated with HCl. As compared in Figure S9, ^{1}H NMR spectrum of P-Im3-

View Article Online
DOI: 10.1039/D5TB00734H

DMSO/HCl mixture shows the peaks in greater than 7 ppm, which could be attributed to the cleavage of partial imine bonds in the presence of acid, which could improv the relaxation of protons in degraded network polymers.

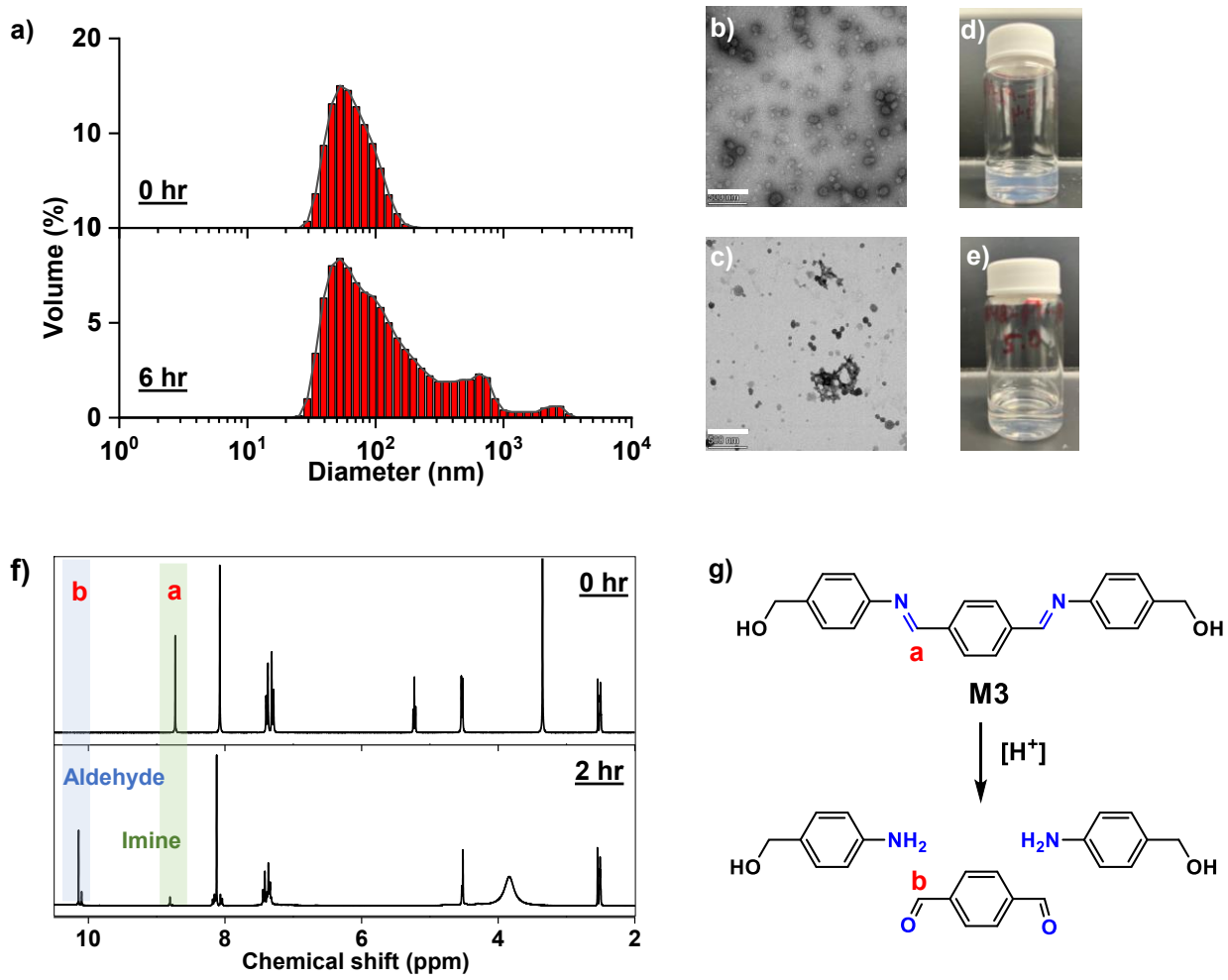

Figure 5. DLS diagrams of aqueous P-Im3-Aq nanogels incubated at pH 5.0 over 6 hrs (a); their TEM images (scale bar = 500 nm) (b,c), and digital images (d,e); and overlaid ^{1}H NMR spectra of M3 in DMSO-d_6/HCl (f) and acid-catalyzed hydrolysis of benzoic imine bond in M3 (g).

Light-Responsive Degradation and Disassembly. The light response of aqueous P-Im3-Aq nanogels was investigated using UV/Vis spectroscopy upon the irradiation of visible light at λ = 440 nm. As seen in Figure 6a, the absorption gradually decreased over irradiation time. The absorbance at λ = 355 nm was monitored to determine %degradation. It decreased to 40% over

View Article Online
DOI: 10.1039/D5TB00734H

24 hrs. Additionally, the DLS diagrams and TEM images show no change in size distribution over the irradiation time, suggesting that only cores could be disintegrated through E/Z isomerization of conjugate benzoic imines, with no chemical cleavages (Figure S10).

To get insight into the plausible mechanism of decrease in absorption, M3 dissolved in DMSO (30 uM) was examined for the light response of the conjugate benzoic imine bonds. As seen in Figure 6b, absorbance at λ = 355 nm decreased to >90% in 24 hrs. Interestingly, maximum absorption wavelength was blue-shifted over irradiation time, which could be attributed to the photochemical E/Z isomerization of two C=N bonds under visible light.[42, 63] Notably, the degradation of P-Im3-Aq nanogels appeared to be slower than that of M3, which is attributed to the delayed penetration of visible light to crosslinked cores in nanogels. Our results obtained from UV/Vis spectroscopic analysis of M3 and P-Im3-Aq suggest that the destabilization of nanogels upon exposure to visible light could be attributed to change in UV absorption due to photo-induced E/Z isomerization.

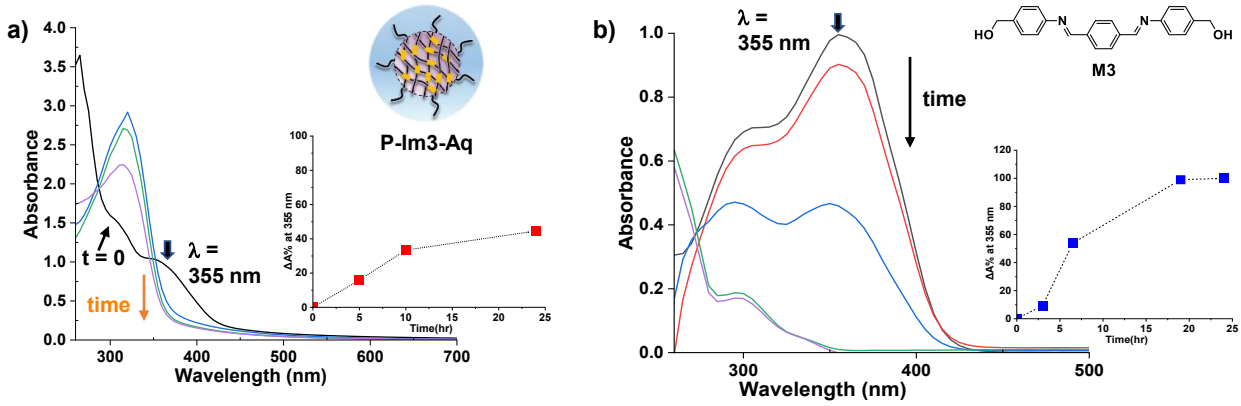

Figure 6. UV/Vis spectra of aqueous P-Im3-Aq nanogels (a) and M3 in DMSO (b) under visible light irradiation at 420 nm over a 24-hour period, with inset plots showing the absorbance changes at 355 nm.

Computational Studies of E/Z Isomerization of M3 by DFT Calculations. M3 labeled with two conjugate benzoic imine bonds could be presented with three ground state configurations as shown in Figure 7a (e.g. EE, EZ, and ZZ). Their transitions as EE → EZ → ZZ are assumed to be achieved through a photo-induced E/Z isomerization of benzoic imine bonds.

View Article Online
DOI: 10.1039/D5TB00734H

We scan the potential energy surface to characterize the ground states of EE, EZ and ZZ configurations of M3 and the transition states TS1 and TS2 for EE → EZ and EZ → ZZ isomerization pathways, respectively. DFT calculations show that EE is the most stable configuration, compared to EZ and ZZ, while ZZ is the least stable configuration. The ground state energy of EE calculated through DFT is 3 kcal/mol and 11 kcal/mol lower compared to EZ and ZZ configurations (Figure S11). The STQN method implemented in Gaussian 16 was used to locate these transition states. Three structure specifications are required in this method: the reactants (EE for EE → EZ and EZ for EZ → ZZ), the products (EZ for EE → EZ and ZZ for EZ → ZZ), and an initial guess for the transition state structure. The estimated activation energy for EE → EZ (ΔG‡EZ) and EZ → ZZ (ΔG‡ZZ) was calculated to be 19 and 21 kcal/mol, respectively.

We use TD-DFT calculations to predict the absorption spectra of EE, EZ and ZZ configurations. The vertical excitation energy for three different configurations of M3 was calculated and the excitation energies, oscillator strength and possible electron transitions are summarized in Table S3 and Figure S12, respectively. Figure 7b shows the absorption spectra of EE (black), EZ (red) and ZZ (blue) configurations calculated via TD-DFT. The calculated λ_{max} = 337 nm for the EE configuration is in good agreement with the experimental result (λ_{max} = 355 nm). The EZ and ZZ configurations had progressively lower absorbance values. The EZ demonstrates a decrease in absorbance and a blue shift, while the ZZ exhibits the lowest absorbance, signifying substantial disruption in the conjugate structure. The similarity in spectral features between experimental and computational studies indicates that the light-responsive degradation of M3 (shown in Figure 6b) could be attributed to stepwise transformation to EZ and ZZ forms upon exposure to light.

Frontier molecular orbital (FMO) is crucial for electrical and optical properties and chemical reactions. Figure S13 shows the HOMO-1, HOMO, LUMO and LUMO+1 of EE configuration. Yellow and cyan regions show FMO with opposite phases. The positive phase of the molecule is represented in yellow color and the negative phase in cyan color. The HOMO is localized mainly on aromatics, while the LUMO is relocated on the whole system. Moreover, electron orbital delocalization can be seen across imine bonds for HOMO. The LUMO is anti-bonding orbital

View Article Online
DOI: 10.1039/D5TB00734H

(π^*) with respect to the C=N which justifies the $\pi \rightarrow \pi^*$ excitation according to FMO of EE configuration.

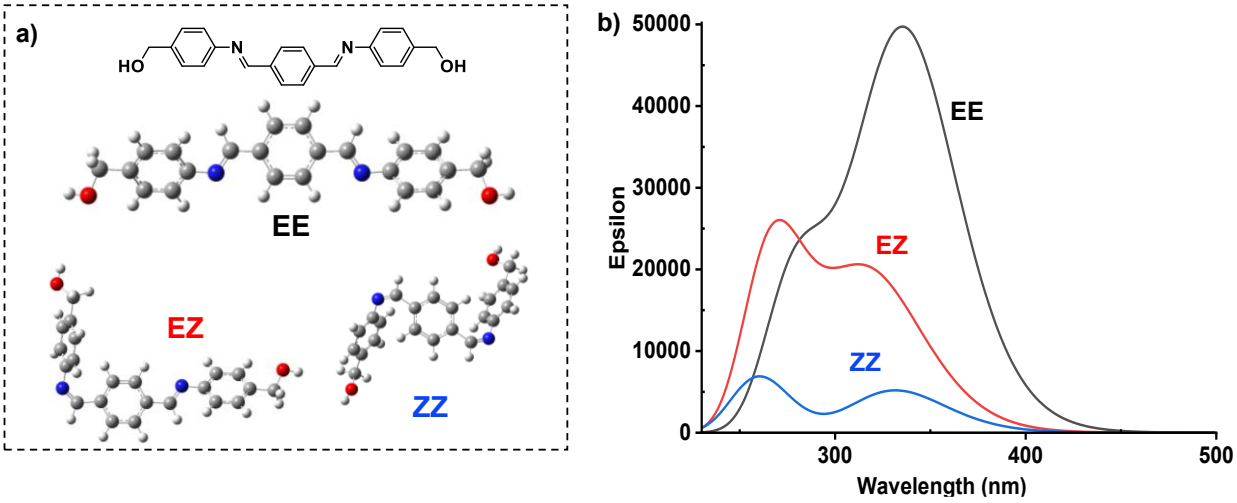

Figure 7. Three M3 configurations as EE, EZ, and ZZ (a) and absorption spectra of EE (black), EZ (red) and ZZ (blue) configurations calculated via TD-DFT (b).

Encapsulation and Dual Acidic pH/Light-Responsive Release of Cur. Cur is a potent bioactive agent with therapeutic effects against various diseases, including cancer.[64, 65] Since being hydrophobic, Cur could be encapsulated in hydrophobic cores of P-Im3-Aq nanogels mainly through hydrophobic-hydrophobic interaction. Here, Cur-loaded aqueous nanogels (P-Im3-Aq/Cur) in colloidally stable, yellow suspension were fabricated by the addition of a solution of Cur in DMSO to aqueous P-Im3-Aq dispersion, followed by purification with dialysis and filtration. With the pre-determined extinction coefficient of Cur (ε = 55,000 $M^{-1}cm^{-1}$) in THF/water (1/1 v/v) (Figure S14) and UV/Vis spectrum of aqueous P-Im3-Aq/Cur dispersion (Figure S15), the loading level of Cur to be 4.7 wt% and its loading efficiency to be 24.5% were determined. DLS analysis reveals that it had an average diameter of 130 nm (Figure 8b).

The fabricated P-Im3-Aq/Cur was next evaluated for *in vitro* release of Cur in acidic pH, upon the irradiation of visible light, and both, using UV/Vis spectroscopy. For light responsive release, aliquots in quartz cuvette were exposed to visible light at λ = 420 nm. Due to poor solubility in water, Cur released from nanogels was precipitated from the solution. UV/Vis spectra of supernatants were recorded for given time intervals (Figure S16). The absorbance at λ

View Article Online
DOI: 10.1039/D5TB00734H

= 430 nm was used to determine the amount of released Cur and thus %release. As seen in Figure 8c, %release significantly increased to reach 80% within 8 hrs. Compared with negligible release of Cur under dark conditions, such enhanced release of Cur under visible light could be attributed to structural change of benzoic imine bonds through photo-induced E/Z isomerization, causing the destabilization of Cur-loaded cores. For pH-responsive release, aliquots were incubated at endo/lysosomal pH = 5.0 and physiological pH = 7.4 for comparison. UV/Vis spectra of supernatant were recorded at given time intervals (Figure S17). As compared in Figure 8d, %release was less than 10% at pH = 7.4 up to 25 hrs, which could be attributed to natural loss. At pH = 5.0, %release increased to 51% in 20 hrs, which could be attributed to acid-responsive degradation of nanogels through acid-catalyzed hydrolysis of benzoic imine bonds. More promisingly, when P-Im3-Aq/Cur was irradicated by visible light in acidic pH = 5.0, % release was synergistically accelerated, reaching 70% within 15 hrs (Figure S18). Such rapid release results from the dual-responsive degradation mechanism, involving both the cleavage of conjugate benzoic imine linkages within the crosslinked core and the destabilization of the core structure through benzoic imine isomerization.

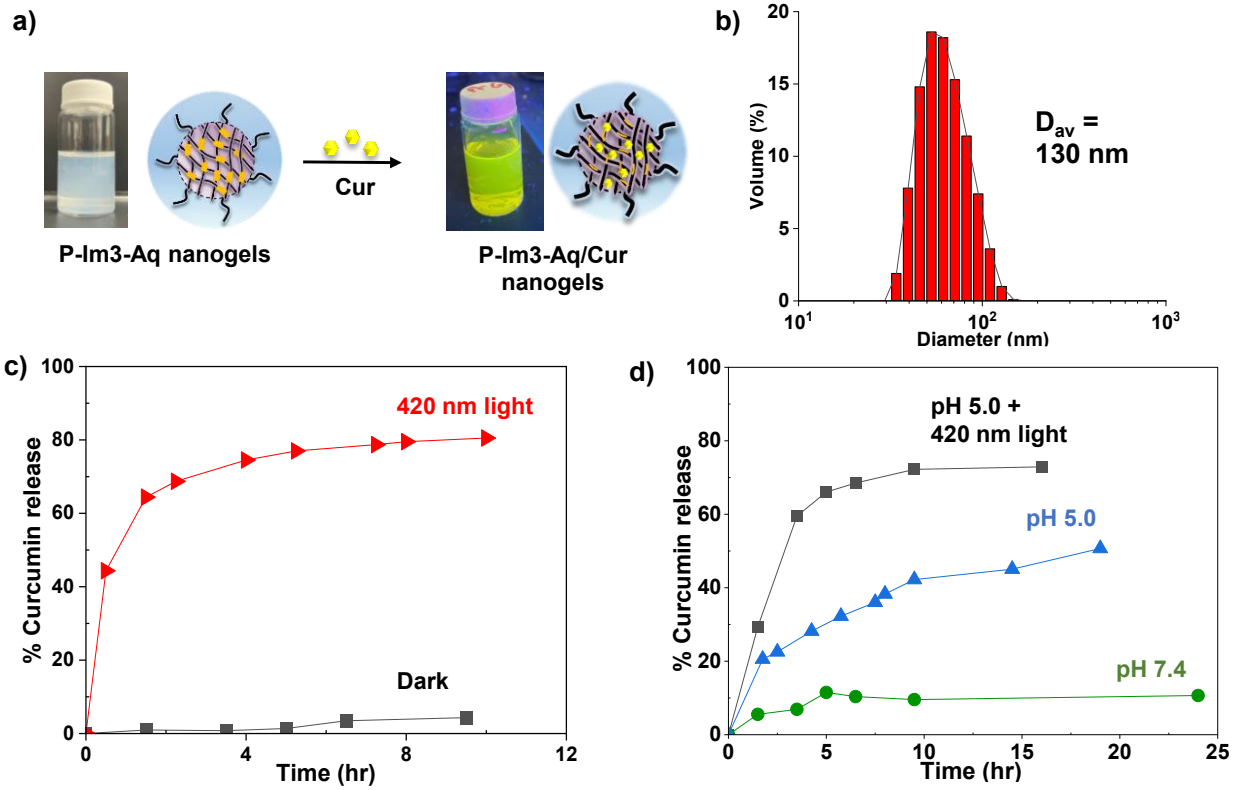

View Article Online
DOI: 10.1039/D5TB00734H

Figure 8. Digital images (upon the irradiation of UV light at 365 nm) and schematic representation of Cur encapsulated in crosslinked nanogels (P-Im3-Aq) to form P-Im3-Aq/Cur nanogels (a), DLS diagram of aqueous P-Im3-Aq/Cur (b), and %release of Cur from P-Im3-Aq/Cur upon irradiation of visible light at 420 nm, compared with in dark as a control (c), and in acidic pH = 5.0, compared in pH = 7.4, as well as both (d), by UV/Vis spectroscopy. Note that light-responsive release experiment (Figure 8c) was done in the greater concentration of P-Im3-Aq/Cur nanogels than acid- and dual-acid/light responsive release experiment.

Intracellular trafficking and anti-tumor activity. Given the promising results with dual acid/light-responsive degradation and Cur release, the P-Im3-Aq/Cur nanogels were evaluated as a mechanism for effective intracellular drug delivery of Cur. Figure 9a shows the viability of HeLa (human cervical adenocarcinoma) cells to be >90% when incubated with empty nanogels up to 240 μg/mL, which suggests that they are not toxic to cells and are biocompatible. As shown in Figure 9b, the viability of HeLa cells decreased to 50% when incubated with increasing concentrations of P-Im3-Aq/Cur nanogels up to 240 μg/mL (equivalent to 11.2 μg/mL). The viability of HeLa cells dropped to below 10% with >5 μg/mL of free Cur, and the IC_{50} was calculated to be 2.72 μg/mL (equivalent to 7.39 μM), which is in the range of literature values (3.36-13.8 μM for HeLa cells).[66, 67] The linear reduction in the viability of HeLa cells with increasing concentrations of P-Im3-Aq/Cur nanogels suggests that there is controlled release of Cur.

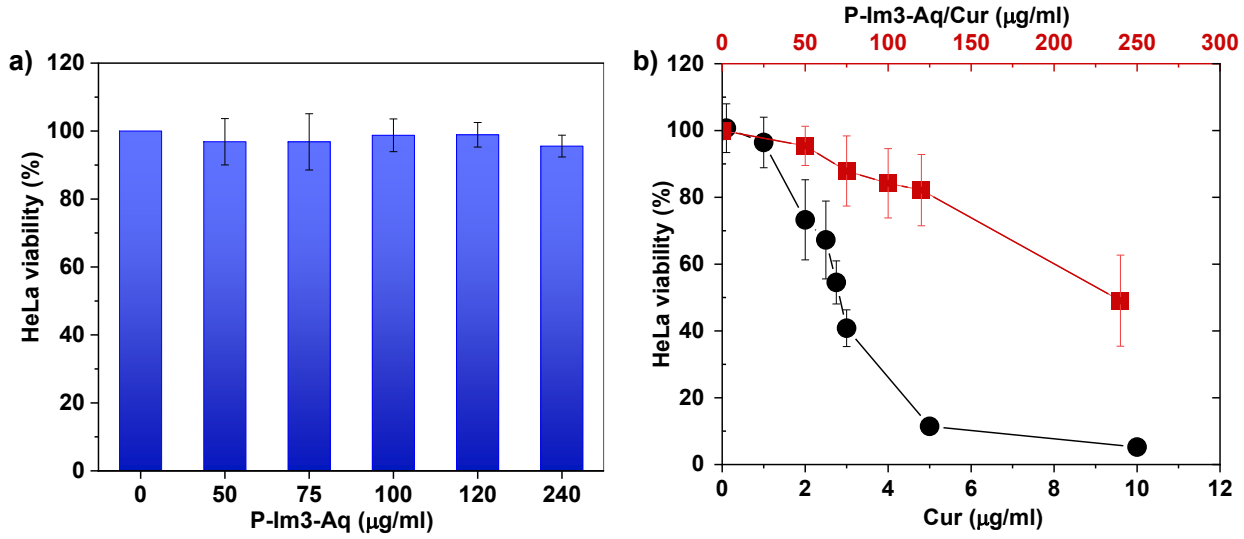

View Article Online
DOI: 10.1039/D5TB00734H

Figure 9. The viability of HeLa cells (%, y-axis) after incubation for 72 hrs with different concentrations of empty P-Im3-Aq nanogels (μg/mL, x-axis) is shown in the bar graph (a). Line graphs show the change in HeLa cell viability (%, y-axis) after incubation with different concentrations of P-Im3-Aq/Cur nanogels (μg/mL, top x-axis, red line) compared with free Cur (μg/mL, bottom x-axis, black line) (b). The averages are shown with error bars as standard deviations for all replicates (n = 9).

Next, the cellular uptake of P-Im3-Aq/Cur nanogels was evaluated in HeLa cells using live-cell imaging with a spinning disk confocal microscope. Figure 10 shows fluorescence images of HeLa cells after incubation with P-Im3-Aq/Cur nanogels for 2 hrs (bottom), compared with empty P-Im3-Aq nanogels (middle) and free Cur (top). The nuclei shown in magenta were stained with SYTO Deep Red Nucleic Acid Stain and Cur fluorescence is shown in green. Free Cur and P-Im3-Aq/Cur nanogels exhibited a distinct perinuclear accumulation, indicating efficient cellular uptake by the endomembrane network. In contrast, cells with empty nanogels showed no detectable fluorescence for Cur. These results support that P-Im3-Aq/Cur nanogels can enter cells allowing for the delivery of Cur.

View Article Online
DOI: 10.1039/D5TB00734H

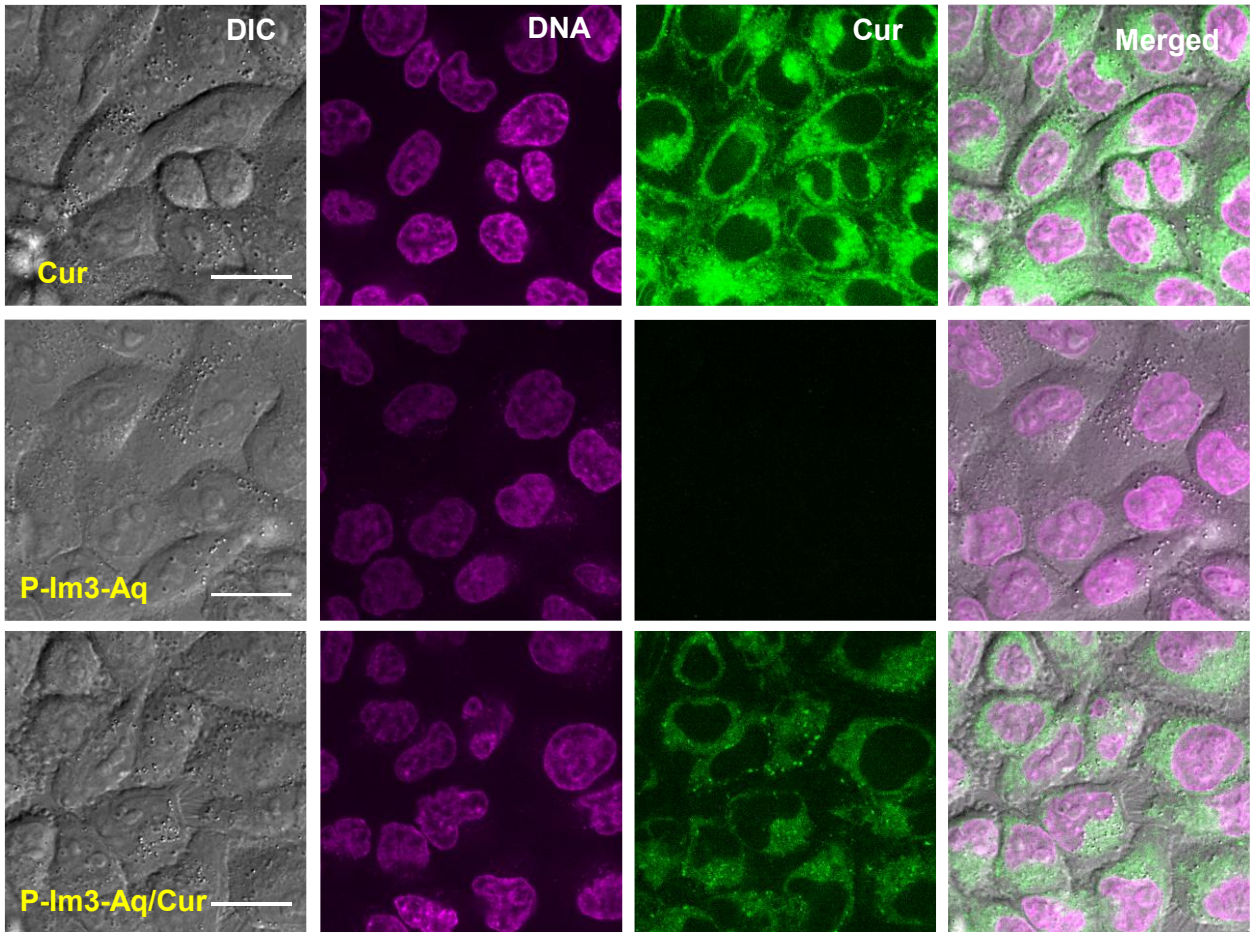

Figure 10. Images show HeLa cells 2 hours after incubation with free Cur (2.72 µg/mL) (top), empty P-Im3-Aq (240 µg/mL; middle), and P-Im3-Aq/Cur nanogels (240 µg/mL; bottom). DIC shows a field of cells, magenta shows the nuclei, green shows Cur, and the merged shows the three channels together. The images for each channel were collected using the same optical settings and similarly processed. The scale bar is 20 µm.

CONCLUSION

We developed a robust approach exploring pre-crosslinking dispersion to fabricate colloidally stable, core-crosslinked nanogels exhibiting dual acid/visible light response with a single extended conjugate aromatic imine bond. A well-defined PEG-b-PCIMA block copolymer synthesized by RAFT polymerization reacted with a novel M3 diol crosslinker bearing extended conjugate benzoic imine bond through a CDI-mediated coupling reaction in an organic solvent.

View Article Online
DOI: 10.1039/D5TB00734H

Following mechanical dispersion of the formed crosslinked polymers in aqueous solution allows for the fabrication of well-defined core/shell nanogels with hydrophobic cores crosslinked through the formation of carbonate linkages, surrounded with hydrophilic PEG corona. The nanogels were spherical with monomodal distribution and were non-cytotoxic. When exposed to acidic pH and visible light, the nanogels (e.g, crosslinked cores) degraded, confirmed by DLS and TEM analyses. Such degradation could be attributed to the acid-catalyzed hydrolysis in acidic pH, while photo-induced E/Z isomerization of aromatic imine bonds upon the irradiation of visible light, confirmed by ^{1}H NMR spectroscopy and computational DFT studies. The nanogels were capable of encapsulating up to 4.6% of the Cur anticancer drug. They exhibited the accelerated and synergistic release of Cur in a combination of acidic pH and visible light, and entered HeLa cells, reducing their viability. Notably, compared to free Cur, the linear reduction in cell viability suggests that Cur was released in a controlled manner, which could be highly desired as a method to reduce the side-effects caused by treatments using free drug. These findings underscore the potential of the core-crosslinked nanogels bearing extended conjugate aromatic imine bonds as a promising platform for dual stimuli-responsive drug delivery, where dual acidic pH and visible light response enable enhanced control for advanced cancer therapy.

ACKNOWLEDGMENTS

This work is supported from Natural Science and Engineering Research Council (NSERC) in Canada through Discovery Grant, Collaborative Research and Training Experience Training (CREATE) Program entitled Polymer Nanoparticles Drug Delivery (PoND), and Canada Research Chair (CRC) Award. JKO was entitled Tier II CRC in Nanobioscience (2011-2021). KK thanks the School of Graduate Studies and Research at Concordia University for Concordia University Graduate Fellowship to support her PhD study. Authors thank Dr. Nooshin Movahed in the Center for NanoScience Research for TEM measurements and Heng Jiang for HR-MS studies. Authors also thank Calcul Quebec, the Digital Re-search Alliance of Canada and the Center for Research in Molecular Modeling (CERMM) for providing computational resources.

View Article Online
DOI: 10.1039/D5TB00734H

REFERENCES

1. M. A. Beach, U. Nayanathara, Y. Gao, C. Zhang, Y. Xiong, Y. Wang and G. K. Such, *Chem Rev*, 2024.
2. A. Harada and K. Kataoka, *Prog. Polym. Sci.*, 2006, **31**, 949.
3. A. S. Mikhail and C. Allen, *J. Controlled Release*, 2009, **138**, 214.
4. N. Nishiyama and K. Kataoka, *Adv. Polym. Sci.*, 2006, **193**, 67.
5. X.-B. Xiong, A. Falamarzian, S. M. Garg and A. Lavasanifar, *J. Controlled Release*, 2011, **155**, 248.
6. J. Ding, L. Chen, C. Xiao, L. Chen, X. Zhuang and X. Chen, *Chem. Commun.* , 2014, **50**, 11274.
7. C. Allen, D. Maysinger and A. Eisenberg, *Colloids Surf., B*, 1999, **16**, 3.
8. S. Taurin, H. Nehoff and K. Greish, *J. Controlled Release*, 2012, **164**, 265.
9. L. Zhang, Y. Li and J. C. Yu, *J. Mater. Chem. B*, 2014, **2**, 452.
10. J. W. Nichols and Y. H. Bae, *Nano Today*, 2012, **7**, 606.
11. Y. H. Bae and K. Park, *J. Controlled Release*, 2011, **153**, 198.
12. O. C. Farokhzad and R. Langer, *ACS Nano*, 2009, **3**, 16.
13. A. Prokop and J. M. Davidson, *J. Pharm. Sci.*, 2008, **97**, 3518.
14. H. Cabral, Y. Matsumoto, K. Mizuno, Q. Chen, M. Murakami, M. Kimura, Y. Terada, M. R. Kano, K. Miyazono, M. Uesaka, N. Nishiyama and K. Kataoka, *Nat. Nanotechnol.*, 2011, **6**, 815.
15. J. Wang, W. Mao, L. L. Lock, J. Tang, M. Sui, W. Sun, H. Cui, D. Xu and Y. Shen, *ACS Nano*, 2015, **9**, 7195.
16. S. Mura, J. Nicolas and P. Couvreur, *Nat. Mater.*, 2013, **12**, 991.
17. C. J. F. Rijcken, O. Soga, W. E. Hennink and C. F. van Nostrum, *J. Controlled Release*, 2007, **120**, 131.
18. Q. Zhang, N. R. Ko and J. K. Oh, *Chem. Commun.* , 2012, **48**, 7542.
19. A. W. Jackson and D. A. Fulton, *Polym. Chem.*, 2013, **4**, 31.
20. Y. Wang, H. Xu and X. Zhang, *Adv. Mater.*, 2009, **21**, 2849.
21. K. Loomis, K. McNeeley and R. V. Bellamkonda, *Soft Matter*, 2011, **7**, 839.
22. A. B. Cook and P. Decuzzi, *ACS Nano*, 2021, **15**, 2068.
23. K. K. Bawa and J. K. Oh, *Mol. Pharmaceutics*, 2017, **14**, 2460.
24. H. Liu, H. H. Lu, Y. Alp, R. Wu and S. Thayumanavan, *Prog Polym Sci*, 2024, **148**.
25. I. F. Tannock and D. Rotin, *Cancer Res.*, 1989, **49**, 4373.
26. P. Watson, A. T. Jones and D. J. Stephens, *Adv. Drug Deliv. Rev.*, 2005, **57**, 43.
27. S. Bazban-Shotorbani, M. M. Hasani-Sadrabadi, A. Karkhaneh, V. Serpooshan, K. I. Jacob, A. Moshaverinia and M. Mahmoudi, *J. Control. Release*, 2017, **253**, 46.
28. S. Binauld and M. H. Stenzel, *Chem. Commun.* , 2013, **49**, 2082.
29. G. Kocak, C. Tuncer and V. Butun, *Polym. Chem.*, 2017, **8**, 144.
30. M. Huo, J. Yuan, L. Tao and Y. Wei, *Polym. Chem.*, 2014, **5**, 1519.
31. Y. Ding, Y. Kang and X. Zhang, *Chem. Commun.* , 2015, **51**, 996.
32. X. Qu and Z. Yang, *Chem. - Asian J.*, 2016, **11**, 2633.
33. A. M. Jazani and J. K. Oh, *Polym. Chem.*, 2020, **11**, 2934.
34. X. Hu, A. M. Jazani and J. K. Oh, *Polymer*, 2021, **230**, 124024.
35. N. Kongkatigumjorn and D. Crespy, *Polymer Chemistry*, 2024, **15**, 4491.

View Article Online
DOI: 10.1039/D5TB00734H

36. J. F. Gohy and Y. Zhao, *Chem Soc Rev*, 2013, **42**, 7117.
37. H. Zhao, E. S. Sterner, E. B. Coughlin and P. Theato, *Macromolecules* 2012, **45**, 1723.
38. Y. Zhao, *Macromolecules* 2012, **45**, 3647.
39. Q. Jin, T. Cai, H. Han, H. Wang, Y. Wang and J. Ji, *Macromol. Rapid Commun.*, 2014, **35**, 1372.
40. A. M. Jazani and J. K. Oh, *Polymer Chemistry*, 2022, **13**, 4557.
41. L. Meng, W. Huang, D. Wang, X. Huang, X. Zhu and D. Yan, *Biomacromolecules*, 2013, **14**, 2601.
42. K. Bairagi, J. T. Liu, A. Thinphang-nga and J. K. Oh, *Macromolecules*, 2023, **56**, 4307.
43. H. S. El-Sawy, A. M. Al-Abd, T. A. Ahmed, K. M. El-Say and V. P. Torchilin, *ACS Nano*, 2018, **12**, 10636.
44. J. K. Oh, *Polym. Chem.*, 2019, **10**, 1554.
45. I. Altinbasak, Y. Alp, R. Sanyal and A. Sanyal, *Nanoscale*, 2024, **16**, 14033.
46. J. Hu, J. He, D. Cao, M. Zhang and P. Ni, *Polym. Chem.*, 2015, **6**, 3205.
47. Z. Zhang, L. Yin, C. Tu, Z. Song, Y. Zhang, Y. Xu, R. Tong, Q. Zhou, J. Ren and J. Cheng, *ACS Macro Lett.*, 2013, **2**, 40.
48. W. Zhu, Y. Wang, X. Cai, G. Zha, Q. Luo, R. Sun, X. Li and Z. Shen, *J. Mater. Chem. B*, 2015, **3**, 3024.
49. B. Liu and S. Thayumanavan, *J. Am. Chem. Soc.*, 2017, **139**, 2306.
50. S.-J. Lee, K.-H. Min, H.-J. Lee, A.-N. Koo, H.-P. Rim, B.-J. Jeon, S.-Y. Jeong, J.-S. Heo and S.-C. Lee, *Biomacromolecules*, 2011, **12**, 1224.
51. W. Chen, M. Zheng, F. Meng, R. Cheng, C. Deng, J. Feijen and Z. Zhong, *Biomacromolecules*, 2013, **14**, 1214.
52. Y. Olszowy, J. Wesselmann, S. F. Over, F. Pätzold and R. Weberskirch, *Polymer Chemistry*, 2023, **14**, 3761.
53. X. Wang, L. Wang, S. Yang, M. Zhang, Q. Xiong, H. Zhao and L. Liu, *Macromolecules*, 2014, **47**, 1999.
54. H. Y. Yang, Y. Li, M.-S. Jang, Y. Fu, T. Wu, J. H. Lee and D. S. Lee, *European Polymer Journal*, 2019, **121**.
55. M. Hartlieb, T. Bus, J. Kubel, D. Pretzel, S. Hoeppener, M. N. Leiske, K. Kempe, B. Dietzek and U. S. Schubert, *Bioconjug Chem*, 2017, **28**, 1229.
56. K. Raghupathi, L. Li, J. Ventura, M. Jennings and S. Thayumanavan, *Polym. Chem.*, 2014, **5**, 1737.
57. X. Hu and J. K. Oh, *Macromol. Rapid Commun.*, 2020, **41**, 2000394.
58. J. D. Chai and M. Head-Gordon, *Physical Chemistry Chemical Physics*, 2008, **10**.
59. M. J. Frisch, J. A. Pople and J. S. Binkley, *The Journal of chemical physics*, 1984, **80**, 3265.
60. D. Tahaoglu, H. Usta and F. Alkan, *J Phys Chem A*, 2022, **126**, 4199.
61. M. Frisch, G. Trucks, H. Schlegel, G. Scuseria, M. Robb, J. Cheeseman, G. Scalmani, V. Barone, G. Petersson and H. J. G. I. W. C. Nakatsuji, 2016, **1**, 572.
62. X. Hu and J. K. Oh, *Macromol Rapid Commun*, 2020, **41**, e2000394.
63. P. J. Coelho, M. C. R. Castro and M. M. M. Raposo, *Journal of Photochemistry and Photobiology A: Chemistry*, 2013, **259**, 59.
64. N. Dhillon, B. B. Aggarwal, R. A. Newman, R. A. Wolff, A. B. Kunnumakkara, J. L. Abbruzzese, C. S. Ng, V. Badmaev and R. Kurzrock, *Clin Cancer Res*, 2008, **14**, 4491.

View Article Online
DOI: 10.1039/D5TB00734H

65. V. Zoi, V. Galani, G. D. Lianos, S. Voulgaris, A. P. Kyritsis and G. A. Alexiou, *Biomedicines*, 2021, **9**.
66. K. K. Gupta, S. S. Bharne, K. Rathinasamy, N. R. Naik and D. Panda, *FEBS J*, 2006, **273**, 5320.
67. R. Rashmi, N. Prakash, H. Narayanaswamy, M. N. Swamy, D. Rathnamma, P. Ramesh, U. Sunilchandra, C. Santhosh, H. Dhanalakshmi, N. Nagaraju and H. Vanishree, *Journal of Entomology and Zoology Studies*, 2020, **8**, 267.

Data availability

View Article Online
DOI: 10.1039/D5TB00734H

The data corrected throughout the course of the study are presented and detailed within the main sections of the manuscript and the ESI.